Novel Applications of Cardiovascular Magnetic Resonance Imaging-Based Computational Fluid Dynamics Modeling in Pediatric Cardiovascular and Congenital Heart Disease

Margaret M. Samyn and John F. LaDisa

Additional information is available at the end of the chapter

Abstract

Cardiovascular diseases (CVDs) afflict many people across the world; thus, understanding the pathophysiology of CVD and the biomechanical forces which influence CVD progression is important in the development of optimal strategies to care for these patients. Over the last two decades, cardiac magnetic resonance (CMR) imaging has offered increasingly important insights into CVD. Computational fluid dynamics (CFD) modeling, a method of simulating the characteristics of flowing fluids, can be applied to the study of CVD through the collaboration of engineers and clinicians. This chapter aims to explore the current state of the CMR-derived CFD, as this technique pertains to both acquired CVD (i.e., atherosclerosis) and congenital heart disease (CHD).

Keywords: computational, modeling, cardiovascular, atherosclerosis, congenital

1. Introduction

Cardiovascular disease (CVD) is a common cause of morbidity and mortality around the world [1]. Each year, CVD afflicts more than 1.9 million in the European Union and at least 800,000 in the United States of America (USA). The cost of health care has been increasing exponentially over the years with estimates noting about 196 billion Euros per year and 207.3 billion dollars spent annually on direct/indirect costs of cardiovascular disease [1]. In the United States, almost 801,000 Americans died from heart disease, stroke, or other CVD in 2013 and ~85.6 million

Americans live with some form of CVD [1, 2]. While far fewer have congenital heart disease (CHD), these structural problems still afflict about 1% of live-born children and many require intricate operations for treatment/palliation. American Heart Association data suggest that approximately two million Americans live with some form of CHD, as do millions of Europeans and other individuals globally [3].

Mechanical stimuli (such as pressure and strain) have been shown to influence the onset and progression of CVD. For example, wall tension can be estimated as the product of vessel radius and blood pressure (BP). Chronic changes in wall tension initially driven by increases in pressure are believed to be the stimuli for vessel thickening, which then restores wall stress to a preferred operating range [4]. Strain also reflects aortic deformation as present with hypertension and aneurysm formation [5, 6].

Of particular interest is wall shear stress (WSS) (**Figure 1**), which can be generally defined as the frictional force exerted on the walls of a vessel as a result of flowing blood. Areas of low time-averaged WSS are known to correlate with sites of atherogenesis and inflammation from prior studies [7–12]. These studies suggest that specific alterations in mechanical stimuli manifesting from CVD may be the stimuli ultimately leading to morbidity. Hence, there is value in knowing how and when they lead to structural, as well as functional and hemodynamic vascular changes.
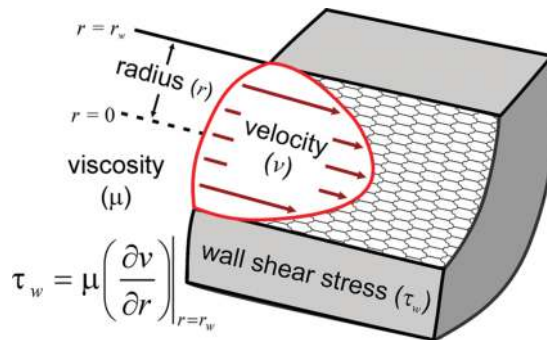

Figure 1. Wall shear stress (WSS). The figure shows schematic illustration of the velocity profile experienced by endothelial cells lining a vessel as a result of flowing blood. WSS (τ_w) can generally be defined as the frictional force exerted on the walls of the vessel. In its simplest form (e.g., plane Couette flow), WSS is the product of viscosity and the near-wall velocity gradient ($\partial v/\partial r$), also known as the shear rate or rate of deformation.

The flow patterns of fluids are governed by partial differential equations that represent conservation laws for quantities such as mass and momentum [13]. Predicting the impact of such flows in biomedical applications, as well as within other scientific disciplines, is time consuming and costly without computational tools. Computational fluid dynamics (CFD) is a method of simulating fluid passing through or around an object, in this case blood vessels, by replacing the partial differential equations with algebraic equations that can be solved numerically using digital computers. There are several open source and commercially available CFD software packages that facilitate the completion of these calculations with user-

friendly interfaces that accept various types of medical imaging data. The workflow for each software package then allows a user to generate hemodynamic results (as presented throughout this chapter) with an appreciation for the governing mathematical equations. However, in performing CFD modeling, there are several important clinical and engineering considerations that should be kept in mind.

The general requirements for studying blood flow for patients with CVD and/or CHD using CFD include first creating a model of the vessel geometry from three-dimensional (3D) medical imaging data. Typically, cardiac magnetic resonance (CMR) or computed tomographic (CT) imaging data are readily available 3D data that provide clear definition of anatomy. CFD also requires prescription of the flow information for the entrance and exit of vessels which is gleaned from phase contrast (PC) velocity-encoded CMR data acquired at these sites. It is also necessary to prescribe the hemodynamic state beyond the borders of the 3D imaging dataset in order to obtain physiologic results (e.g., setting downstream resistance to obtain a realistic range of pressure). Direct or indirect assignment of this inlet and outlet information is referred to as "setting the boundary conditions." Rheological properties, such as blood density and viscosity, are then assigned. The last step in the process entails the use of a powerful computer or cluster of computers to solve the governing equations for fluid flow throughout a version of the vessel's geometry, which is represented as a computational mesh.

More specifically, the first step when performing CFD involves creating a computer aided design (CAD) model within the vascular regions of interest from medical imaging data. The CMR imaging focus of the current work most often uses data from either breath-held electro-cardiographically (ECG)-gated, magnetic resonance angiography (MRA) or a respiratory-navigated, ECG-gated 3D nongadolinium-enhanced, entire heart CMR sequence. CFD can be used with other sequences and imaging modalities as well. The models created can provide the geometry on a patient-specific basis when it is desirable to focus on a clinical question for a specific patient, or for a group of patients with similar pathology [14]. Alternatively, representative or idealized models are also sometimes used, where the geometry within the idealized model is informed by measurements taken from data within a collection of CMR scans across one or more patients. To date, our workflow has primarily used SimVascular (simvascular.github.io, latest version, La Jolla, CA, USA), but other commonly used software packages that facilitate the import and segmentation of CMR data include Cardiovascular Integrated Modeling and Simulation (CRIMSON, www.crimson.software), the Vascular Modeling Toolkit (VMTK, www.vtnk.org), and Mimics (biomedical.materialise.com/mimics, Plymouth, MI, USA), just to name a few. Each of these programs then facilitates discretization of the CAD model created from CMR data by interacting with some type of meshing software (e.g., MeshSim, www.simmetrix.com, Clifton Park, NY, USA). The parameters selected during the segmentation and meshing steps used in creating a computational version of the vasculature from CMR can have a large impact on the results obtained. For example, the accuracy of WSS indices (see below for details on specific WSS indices of interest) depends greatly on vessel radius, and therefore on the confidence with which segments or 3D boundaries for the CAD model are created from CMR data. In its simplest form (e.g., plane Couette flow), WSS is the product of viscosity and the near-wall velocity gradient (**Figure 1**) [10]. This change in velocity

from the wall of an artery to the next nearest location is largely determined by details of the computational mesh that are established. Note that the velocity on the wall is often zero due to a no-slip condition. Unfortunately, the computational costs of obtaining CFD results increase as a function of mesh density. The trade-off is often managed in today's CFD studies by using adaptive-meshing approaches [15, 16] yielding smaller meshes that strategically place more elements where they are most needed, such as near the wall, for improved accuracy when determining WSS.

In practice, the density for blood is typically selected from the literature, and a Newtonian assumption (i.e., constant blood viscosity) is most often employed. Although blood is a shear-thinning fluid, meaning that its viscosity decreases as it is deformed, approximating its behavior as Newtonian is generally thought to be reasonable for the range of shear rates experienced by the portions of the vasculature that are highlighted in the CFD studies below. A unique aspect of CFD software packages designed specifically for biomedical applications is their ability to implement boundary conditions that replicate normal and CVD physiology [17]. For example, the time-varying opposition to blood flow (i.e., impedance spectra) can be calculated from pressure and flow measurements made at the same location in the vascular system, but Windkessel models are often used as an approximation of the impedance given the impracticality of the necessary measurements within a clinical setting [17]. It is an increasingly common CFD modeling standard to employ three-element Windkessel representations derived from CMR-acquired PC velocity-encoded (VENC) flow data for inlet and outlet boundary conditions. More recent boundary condition advancements include cardiac function through the use of closed-loop lumped-parameter networks (LPNs) with CFD models. Closed-loop LPNs were initially developed to model single ventricle physiology [18] and are now being used to characterize flow patterns in the coronary arteries and other vascular regions. These closed-loop LPN models are often tuned to match measured clinical data (i.e., cardiac output (CO), stroke volume, blood pressure, and ejection fraction), and then coupled to patient-specific simulations that use specialized computers to solve the conservation of mass, balance of momentum, and (in some cases) the vessel wall elastodynamics equations [19]. The results are vascular hemodynamic indices that may aid the understanding and care of CVD, following detailed analysis of the resulting indices.

The application of CFD to clinical cardiovascular problems typically requires teamwork between clinicians and engineers, with a step-wise approach to gather and analyze specific data for the study of clinically important blood flow issues (**Figure 2**). As an example, understanding flow in the aortic arch by CFD requires CMR data for the anatomy of interest (MRA or other 3D data), as well as blood flow measurements (from PC velocity-encoded magnetic resonance imaging sequence, PC-MRI) for all major inflow and outflow vessels (in this case, the ascending and descending aortic flow, as well as the brachiocephalic vessels, as denoted by the black dotted lines in **Figure 2**). Blood pressure measurements from each limb are also used in assigning boundary conditions.

When creating CFD models for the aortic arch, the inlet is most often aortic flow. Typically, this can be imposed in one of several representations including plug flow (i.e., uniform flow), parabolic flow (as shown in **Figure 1**), or a patient-specific flow obtained from CMR phase

contrast velocity-encoded (PC-MRI) data that intrinsically incorporates elements of both. In vivo, the velocity profile is determined by a ratio of inertial (i.e., those forces driving the flow) to viscous (those forces impeding the flow) forces [17]. If the impact of viscous forces is large, such as in a smaller artery with lower velocity, then the velocity profile will be parabolic. However, in a larger artery such as the aorta, inertial forces are more pronounced, leading to a more uniform velocity profile except near the walls where the impact of viscous forces manifests. It is, therefore, desirable to use a retrospective ECG-gated phase contrast velocity-encoded sequence to sample the velocity profile, which should intrinsically capture these features, downstream of the valve for direct input into a CFD model, but this requires appropriate through-plane and in-plane velocity encoding to adequately resolve flow features. This approach may also be difficult to implement within the typical imaging time available for a clinical case, as it requires specialized sequences and obtains data that are more detailed than that commonly used in clinical imaging. An alternative approach is to construct CFD models with their inlet beginning at the aortic annulus, impose the measured blood flow waveform as an assumed velocity profile at the model inlet (with plug profile or patient-specific flow profile), and allow the curvature and related geometry of the arch to influence the resulting flow patterns [14]. This approach does not require specialized sequences, minimizes the introduction of noise at the model inflow due to inadequate velocity encoding, and allows for improved temporal resolution compared to three-component PC-MRI, using multiple planes for flow assessment [20].
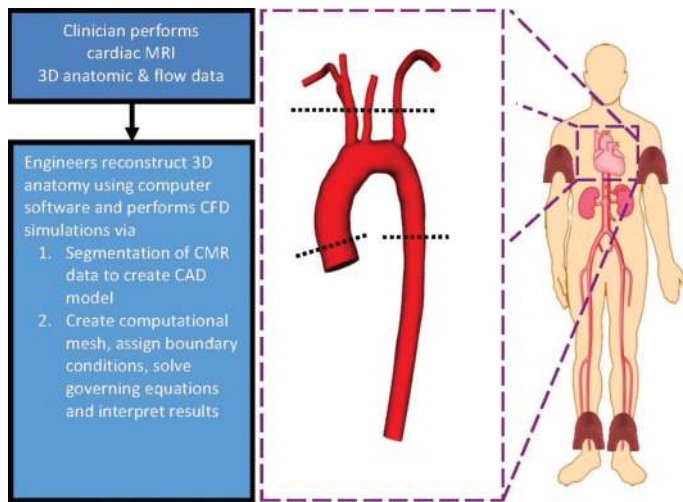

Figure 2. Step-wise creation of computational fluid dynamics (CFD) models. Flow assessments are performed by phase contract magnetic resonance imaging (PC-MRI) at locations noted in the middle panel, while four limb blood pressure assessments are performed after scanning.

In our workflow for CFD simulations of the thoracic aorta to date, which is shown schematically in **Figure 2**, outlet boundary conditions have used measured BP and the PC-MRI flow

data from each brachiocephalic vessel and the descending aorta together with an approach called the "pulse pressure method" to assign elements to the Windkessel parameters [21, 22]. The regional resistances, arterial capacitances, and distal resistances are estimated for each case and used in patient-specific modeling (**Table 1**) [23]. Given the very small nature of the intercostal arteries, and the fact that their flow distributions are not typically characterized by imaging, these are not usually employed in the modeling. While flow to the intercostal arteries is important physiologically, characterizing the flow distributions requires multiple phase contrast image acquisition frames or 4D (four-dimensional) blood flow imaging using CMR that is often beyond the time available and needs of the clinically ordered session.

		Control	T1DM
Young's modulus	E (dyn/cm^2)	3.99E+06–3.57E+07	3.23E+06–1.17E+07
Innominate artery	Rc (dyn·s/cm^5)	429–489	320–939
	C (cm^5/dyn)	1.22E–04–1.42E–04	1.23E–04–3.99E–04
	Rd (dyn·s/cm^5)	4250–6500	4520–9260
Left common carotid artery	Rc (dyn·s/cm^5)	687–1720	702–1390
	C (cm^5/dyn)	3.91E–05–1.15E–04	4.94E–05–1.52E–04
	Rd (dyn·s/cm^5)	10,800–19,600	11,800–15,200
Left subclavian artery	Rc (dyn·s/cm^5)	662–1830	500–1480
	C (cm^5/dyn)	6.11E–05–1.26E–04	6.19E–05–1.62E–04
	Rd (dyn·s/cm^5)	6400–23,000	6813–15,000
Descending aortic outlet	Rc (dyn·s/cm^5)	99–231	101–232
	C (cm^5/dyn)	2.67E–04–8.76E–04	2.84E–04–8.16E–04
	Rd (dyn·s/cm^5)	894–4580	1530–4710

With permission and adapted from Samyn et al. [23].

Table 1. Resistances and capacitances used for CFD simulations of adolescent patients [22].
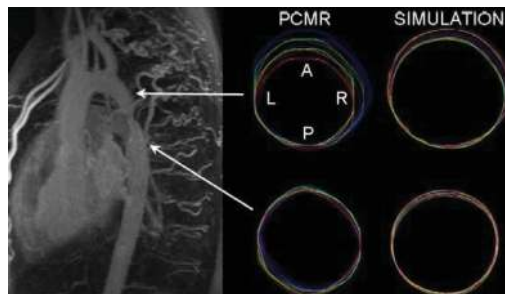

Figure 3. Computational fluid dynamics (CFD) modeling with realistic deformations. A mean intensity projection magnetic resonance angiogram from a patient with aortic coarctation is shown on the left. Temporal wall motion proximal and distal to the coarctation from phase contrast magnetic resonance imaging (PC-MRI) are shown in the middle column, and patient-specific CFD simulations (R = right, L = left, A = anterior, P = posterior) are shown at right.

Fluid-structure interaction (FSI) simulations represent a specialized version of CFD modeling that considers the pulsatility and elastic nature of the arterial system. FSI, therefore, has the potential for introducing more clinically relevant features when determining indices such as instantaneous WSS, time-averaged WSS, and oscillatory shear stress, by including more realistic local deformations (**Figure 3**). For example, considering again the simple case of WSS calculated as the product of the near-wall velocity gradient and viscosity, the movement of the vessel wall as occurs in vivo will impact this calculation. Including local deformations in WSS calculations therefore has the potential to provide more realistic results.

Indices of WSS are calculated from the time-varying velocity field representing flow patterns within the aorta. Blood flow in the aorta, for instance, has long been recognized to be helical and can be replicated by CFD (**Figure 4**) [24]. A helical flow pattern has many positive features including (1) facilitating blood flow transport and suppressing turbulent blood flow, (2) preventing the accumulation of atherogenic low-density lipoprotein (LDL) particles on arterial luminal surfaces, (3) enhancing oxygen transport from the blood to the multilayered arterial wall, (4) reducing the adhesion of platelets and monocytes on the arterial surface, and (5) optimizing flow patterns within origins of the brachiocephalic vessels [25]. Helical blood flow patterns may therefore aid in protecting the arteries from the pathologic mechanisms of atherosclerosis, thrombosis, and intimal hyperplasia, as well as from dilation, aneurysm formation, and dissection [25].
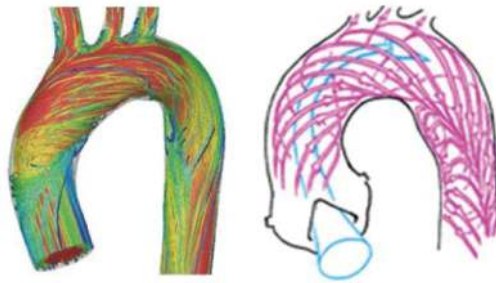

Figure 4. Helical aortic flow. Velocity streamtubes are shown during systole from the simulation of a patient with normal thoracic aortic anatomy (left). The streamtubes replicate the classic patterns elegantly described by Kilner et al. (right) including axially oriented flow during early systole, the development of right-handed helical flow during mid-systole facilitating delivery of blood flow to the arteries of the head and neck, and the presence of complex recirculation regions beginning at end systole [24]. With permission from Wolters-Kluwer journals; Kilner et al. [24].

CFD may offer predictive capabilities for difficult clinical problems as will be discussed in this chapter. For example, MRI during exercise has been pursued since the late 1990s, but is not trivial to implement and is therefore not conducted routinely. More specifically, CMR has been used to quantify blood flow during supine cycle ergometry in the ascending aorta, pulmonary artery [26, 27], abdominal aorta [28, 29], and left ventricle [30]. Indices of WSS and cardiac output were quantified in combination with CFD modeling from a recumbent cycling protocol developed for imaging of the abdominal aorta [31–33]. CFD was also used for patient-specific models of blood flow in the thoracic aorta to quantify indices of WSS under simulated exercise

conditions using changes in blood flow and resistance estimated from various literature sources [34, 35]. More recent exercise protocols for use with CMR go one step further. A pilot study developed a protocol to obtain PC-MRI blood flow measurements in the thoracic and brachiocephalic arteries during a three-tiered supine pedaling, and then related these measurements to noninvasive tissue oxygen saturation levels acquired with near-infrared spectroscopy (NIRS) during assessment using the same protocol [36]. The goal of this work was to use NIRS data as a surrogate for exercise PC-MRI data when setting boundary conditions for future CFD studies of the thoracic aorta under simulated exercise conditions. Relationships and ensemble-averaged PC-MRI inflow waveforms are provided in an online repository for this purpose [36].

There are several indices of WSS that have been associated with locations of atherosclerosis in various vascular beds. The most common of these is time-averaged WSS. WSS is actually represented by vectors that change with each fraction of time within the cardiac cycle. Most reports simply present time-average representations on the wall within the region of interest; this is done for simplicity and because the mechanisms and details by which a particular WSS index leads to neo-intimal thickening are not yet precisely known. Areas of low time-averaged WSS have also been found in a rotating pattern down the descending aorta [37], correlate with areas of plaque deposition [38], and are accentuated after correction of CoA [14]. However, there is evidence suggesting that temporal and spatial changes in WSS may also serve as stimuli for neo-intimal thickening. Oscillatory shear index (OSI) is also commonly reported in CFD studies [11]. OSI is a measure of WSS directionality in which lower OSI values indicate that WSS is oriented predominantly in the primary direction of blood flow, while a value of 0.5 is indicative of bidirectional WSS with a time-average value of zero. Theoretically, regions of low WSS magnitude and high OSI are less likely to experience fluid forces that promote washout of noxious and potentially atherogenic materials in contact with the arterial surface (e.g., LDL). In general, adverse values for these WSS indices (e.g., ~15 dyn/cm^2 for the thoracic aorta) are expressed as thresholds for low magnitude instantaneous and time-averaged WSS. OSI greater than 0.1 are considered adverse, as are spatial and temporal WSS gradients greater than 100 dyn/cm^2 and ±200 dyne/cm^2/s, respectively) [12, 21, 39, 40]. Understanding these hemodynamic principles and differences between indices that use them, the practitioner may apply CFD modeling to describe blood flow patterns in the setting of typical clinical cardiovascular pathology—atherosclerosis and congenital heart disease.

Any discussion of CFD for use in generating flow patterns and indices of WSS would be remiss without a discussion of potential limitations, particularly with respect to advancements in CMR that have facilitated quantification of the same indices through direct processing of data from a more advanced clinical imaging session. For example, 4D blood flow imaging using CMR has been used to investigate flow disruptions in the thoracic aorta [37, 41, 42]. These methods do require specialized pulse sequences that may be outside of the clinical workflow for some centers, are complex to acquire and post-process, and prolong scan time (~15–20 min for a 4D-navigated flow-imaging dataset). Additionally, these methods suffer from low spatial/temporal resolution relative to CFD simulations, which could limit the precision of the WSS results compared to those WSS data calculated from a properly conducted CFD simulation

where uncertainties in the processes employed were appropriately considered [43–45]. For example, the limitations and variability in the model creation process must be carefully controlled by acquiring a high-resolution 3D representation of the anatomy (by MRA or equivalent sequence) and PC-MRI data. Furthermore, the individuals building CAD models must be rigorous when using software, especially with regard to selection of a mesh of sufficiently high density. In this manner, there can generally be a high level of confidence in the results assuming that physiologic boundary conditions have been implemented. WSS results from 4D blood flow imaging can suffer from the same potential limitations of traditional CFD modeling techniques, if the spatial resolution and post-processing operations do not carefully capture the near-wall velocity gradient.

Additional limitations may exist when CFD modeling is attempted for biologic systems. First, clinical acquisition of suboptimal 3D anatomic data can adversely affect models. Acquisition of non-robust 3D data may lead to oversimplification of anatomy during modeling. Second, suboptimally acquired PC-MRI flow data, with inadequate temporal resolution or low dynamic range, may underestimate flow. Third, ignoring cardiac motion, which can affect the accuracy of flow determinations, may lead to errors in modeling [46]. Finally, assigning accurate boundary conditions (especially resistances of the peripheral vasculature or the microcirculation when coronary modeling is attempted) can be challenging, as detailed information may have to be gleaned from the literature because patient-specific data may be difficult to attain. Such resistances can also vary over time and certainly may differ in healthy and diseased states [47].

2. Computational fluid dynamics modeling applied to the study of atherosclerosis

Atherosclerosis is a complex pathobiologic process which begins with endothelial dysfunction, involves a cascade of particles (including white blood cells, chemotactic factors, and smooth muscle cells), and leads to progressive changes in blood vessel walls (**Figure 5**) [48].

After the initial endothelial dysfunction, atherosclerotic plaque develops over many years [49, 50]. The initial feature in the evolution of plaque, seen on autopsy in children as young as 10–18 years old, is the fatty streak [51]. Many studies have shown that intimal thickening, as assessed by ultrasound, can be detected as plaque burden increases. At first, plaque causes outward remodeling of a blood vessel, maintaining the lumen's dimensions, followed by plaque encroachment on the vessel lumen [52]. By the time atherosclerotic plaque causes stenosis (and decreases luminal dimensions by 60% or more), symptoms can be seen under conditions of great oxygen demand, such as exercise. Thus, if the carotid vasculature is affected, cerebral transient ischemic attacks might be manifested, whereas if the coronaries are affected, then myocardial ischemia can occur and be manifested as angina. Peripheral plaque can lead to symptoms of left pain—either claudication or rest pain.
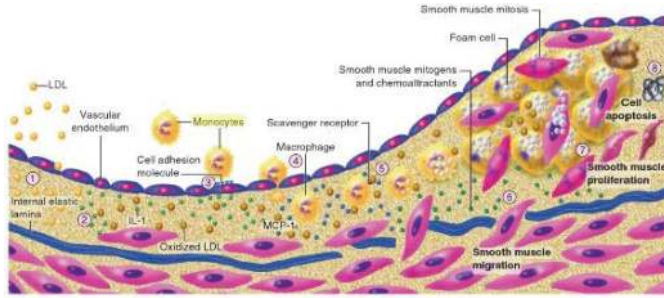
Figure 5. Atherosclerosis. Schematic representation of the evolution of the atherosclerotic plaque. (1) Accumulation of lipoprotein particles in the intima. The modification of these lipoproteins is depicted by the darker color. Modifications include oxidation and glycation. (2) Oxidative stress, including products found in modified lipoproteins, can induce local cytokine elaboration (green spheres). (3) The cytokines thus induced increase the expression of adhesion molecules (blue stalks on endothelial surface) for leukocytes that cause their attachment and chemoattractant molecules that direct their migration into the intima. (4) Blood monocytes, on entering the artery wall in response to chemoattractant cytokines, such as monocyte chemoattractant protein 1 (MCP-1), encounter stimuli such as macrophage colony-stimulating factor (M-CSF) that can augment their expression of scavenger receptors. (5) Scavenger receptors mediate the uptake of modified lipoprotein particles and promote the development of foam cells. Macrophage foam cells are a source of mediators, such as further cytokines and effector molecules such as hypochlorous acid, superoxide anion (O_2^-), and matrix metalloproteinases. (6) Smooth muscle cells (SMCs) migrate into the intima from the media. (7) SMCs can then divide and elaborate extracellular matrix, promoting extracellular matrix accumulation in the growing atherosclerotic plaque. In this manner, the fatty streak can evolve into a fibrofatty lesion. (8) In later stages, calcification can occur (not depicted) and fibrosis continues, sometimes accompanied by SMC death (including programmed cell death, or apoptosis) yielding a relatively acellular fibrous capsule surrounding a lipid-rich core that may also contain dying or dead cells and their detritus (IL-1 = interleukin-1; LDL = low-density lipoprotein) [48]. With permission from Elsevier Health Science.
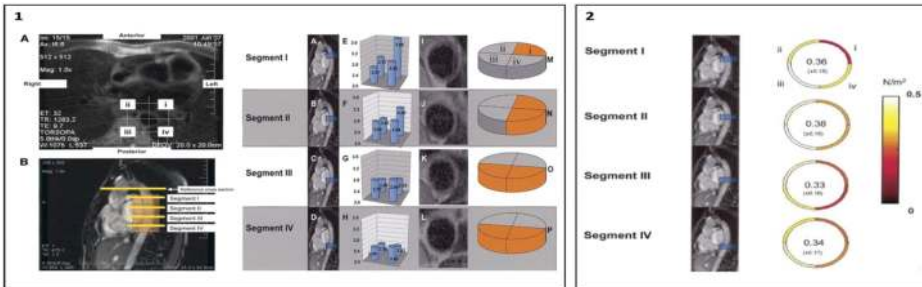

Figure 6. Shear stress and plaque distributions depend on axial and circumferential location. In the upper corner of panel 1, Image A shows circumferential designation (i–iv), while the lower left image (Image B) shows each axial location of the aorta studied. Plaque distribution is shown as pie charts for each segment. On the right (panel 2), shear stress is shown [38]. With permission from Wentzel et al. [38].

Studies have emerged to characterize the vascular hemodynamic effects of plaque by employing computational modeling based on CMR data. This area of CFD research attempts to systematically study vascular WSS and OSI as a way to better understand where plaque forms and how plaque influences blood flow. In a study of adults with preexisting aortic plaque, for

example, time-averaged WSS patterns existed in a rotating pattern down the thoracic aorta that correlated with areas of atherosclerotic plaque [38]. WSS distribution, therefore, depended on the axial level and circumferential location in a given axial level of the aorta (**Figure 6**). Similarly, many other CFD studies have shown low WSS and high OSI are associated with atherosclerosis. In an adult coronary CT study, coronary segments with established plaque exhibited lower WSS compared to adjacent normal areas [53]. Within plaques, WSS was lower, and plaque volume was higher in mid-plaque compared to upstream and downstream areas (**Figure 7**) [53]. In a study of carotid atherosclerosis, low time-averaged WSS and high OSI were seen in areas of increased mature plaque volume (**Figure 8**) [54].
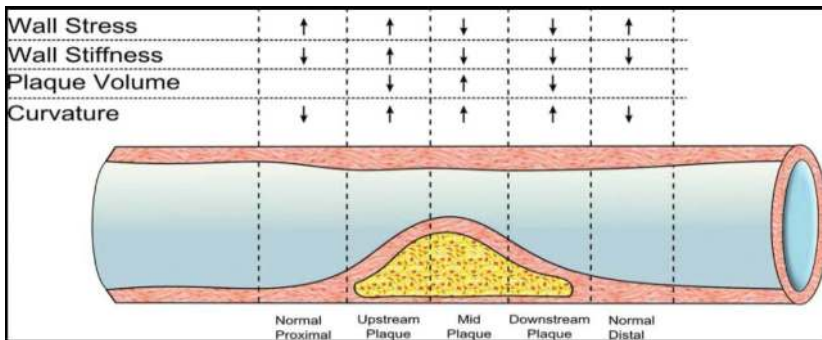

Figure 7. Variation of wall stress (WS), wall stiffness, plaque volume, and curvature along a plaque (note that within plaques, wall shear stress was lower and plaque volume higher in mid-plaque compared to upstream and downstream areas) [53]. With permission from Katranas et al. [53].
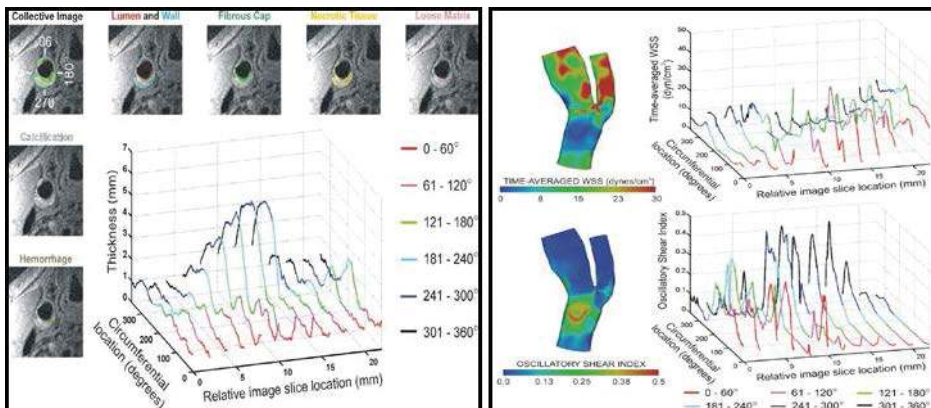

Figure 8. Carotid plaque and wall shear stress. In areas of mature plaque (left), low time-average wall shear stress (right, top right) and high oscillatory sheer index (right, bottom right) are seen [54]. With permission and adapted from LaDisa et al. [54].

This prior work served as motivation for a novel pilot CMR study of early vascular changes in pediatric patients with type 1 diabetes. Twenty preadolescent and adolescent patients with type 1 diabetes (median age of 15.8 years, range of 11.6–18.4 years) were enrolled in this prospective CMR study and compared with eight control subjects (15.8 years with a range of 10.3–18.2 years). Using same-day brachial artery reactivity testing, lower flow-mediated dilation was seen for the subjects with diabetes ($p = 0.036$), as expected—indicating the presence of endothelial dysfunction in this group, as seen by others [55]. When patient-specific CFD models were created from CMR data, those with diabetes had more aortic regions with high time-averaged WSS when compared with controls, although the groups had similar OSI (**Figure 9**) [23]. Many cardiovascular risk factors, including type 1 diabetes, induce physiological outward arterial remodeling (dilation) that begins in response to overall higher initial laminar shear stress (Glagov phenomenon). With vascular inflammation, remodeling progresses, resulting in adverse shear stress in larger arteries [56]. This pilot pediatric diabetes study may provide a glimpse into early vascular remodeling (i.e., where wall shear stress is still high and the aorta, which has begun to stiffen, has yet to dilate). Longitudinal studies are needed to understand how areas of WSS and OSI change with aging, and as atherosclerosis progresses. Understanding this may enhance therapies for early treatment of atherosclerosis by aiding the development of medications that favorably alter WSS and OSI [23].
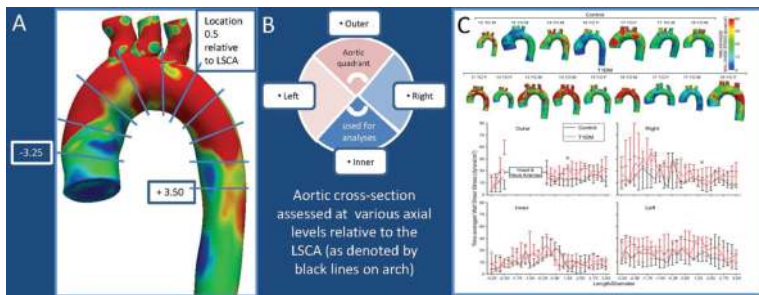

Figure 9. Regional differences in time-average wall shear stress for children with type 1 diabetes (red line) versus controls (black line) are shown (graphs in panel C). Panel A shows the time-averaged wall shear stress (TAWSS) display for a representative patient with type 1 diabetes (T1DM) with blue lines showing where assessments were made relative to the left subclavian artery (LSCA). Panel B shows the circumferential locations assessed. These are displayed graphically in panel C. Along right, left, outer, and, to a lesser degree, the inner curvatures of the aorta, the median time-averaged wall shear stress (TAWSS) at each location for diabetics (red line on the graphs) tended to be higher than median TAWSS for controls (black line), reaching significance at two locations, one along the outer curvature (location 1.25) and another along the anatomic right side (location 1.5) of the aorta [23]. With permission and adapted from Samyn et al. [23].

3. Computational fluid dynamics modeling and congenital heart disease

CFD modeling is useful in understanding not only blood flow as it relates to atherosclerosis but also blood flow in a number of structural heart diseases, including aortic coarctation (CoA),

aortic dilation, and aneurysms (as with bicuspid aortic valve and connective tissues diseases), and for more complex diseases, such as repaired Tetralogy of Fallot (TOF) (to aid percutaneous interventions) and single ventricle physiology (to optimize the Fontan operation's total cavo-pulmonary palliation). Collaboration between clinicians and engineers is important, so that optimal workflow can be achieved to allow timely, patient-specific model creation for consideration in clinical decision making. **Table 2** shows some situations where CFD simulations have been applied to clinical cardiovascular medicine; these will be discussed here.

Area of interest	Applications	Clinical impact	Limitations
Coronary artery disease (CAD)	Models based on angiography or CT scan may predict hemodynamically important plaque.	Models allow virtual stenting to optimize treatment.	Accurate coronary vessel reconstructions and patient-specific boundary conditions (myocardial resistance) are challenging to simulate.
Aorta Aneurysm Dissection Coarctation	Models quantify hemodynamics to develop optimal therapy and predict outcome.	Models may be used to predict aneurysm progression and risk of rupture and may aid in patient follow-up by reducing additional imaging. Models may aid care by allowing appropriate planning and may contribute to stent design.	Wall motion and low image contrast between vessel wall and thrombus may affect modeling, but fluid structure interaction (FSI) may aid analyses.
Arterial wall	Models determine local wall shear stress (WSS) and oscillatory shear index (OSI) related to atherosclerosis.	Models may predict plaque, note sites likely of rupture, and allow optimization of therapy with medications/devices (i.e., stents).	Detailed anatomy of some circulations may be challenging to model; using accurate boundary conditions can be challenging.
Congenial Heart Diseases Coarctation Single ventricle Tetralogy of Fallot	Models aid understanding of blood flow in complex heterogeneous diseases and may aid therapy.	Modeling will allow prediction of hemodynamic response to possible surgical- and device-based treatments which sometimes dramatically alter the circulation.	Some have cited this as the "ultimate personalization challenge" given the heterogeneous nature of each category of CHD, the complex anatomy, and patient-specific boundary conditions needed.

With permission and adapted from Morris et al. [47].

Table 2. Applications of CFD modeling to cardiac disease [46].

3.1. Aortic CFD modeling for congenital heart diseases

Building upon the CFD modeling efforts summarized above that focused on the thoracic aorta as a vascular surrogate for the coronaries in the study of atherosclerosis, CFD modeling research naturally extended to the diseases of the thoracic aorta—especially to the study of CoA. CoA is a relatively common congenital narrowing of the proximal thoracic aorta, occurring in about 8–11% of patients with CHD, and usually involves the thoracic aorta just after the origin of the left subclavian artery (juxta-ductal CoA). Patients with unrepaired CoA may suffer from ill-effects of hypertension (or in infancy, from cardiovascular collapse with ductal closure). Even after successful CoA repair, many are followed due to the presence of bicuspid aortic valve (up to 85%) with or without stenosis, residual hypertension (7–33% of patients) [57], re-coarctation (5–50%) [58], aortic aneurysm, aortic dissection, and possibly early atherosclerosis [59]. Recent CFD modeling studies have shown altered time-average WSS after end-to-end anastomoses [14]. CFD modeling has also been employed to assess WSS after Dacron patch repair of CoA [60]—an operative procedure now known to be complicated by aneurysm formation. Aneurysms, in turn, introduce local geometric abnormalities leading to heterogeneity in WSS that have historically been linked to adverse consequences such as cellular proliferation and plaque progression (**Figure 10**). Bicuspid aortic valve is a frequently found coexisting CHD for patients with CoA—occurring in up to 85% of these individuals. Recently, sophisticated CFD simulations, using a custom MATLAB® program (MathWorks, Natick, MA, USA) to facilitate segmentation of a common variant (right-left cusp fusion) of bicuspid aortic valve, attempted to account for the influence of the valve on flow patterns and turbulence in the ascending aorta [61]. This represents an added step toward realism, and constitutes an alternative to imposing measured PC-MRI data directly when creating patient-specific CFD models for patients with CoA and bicuspid aortic valve. Additionally, attempts to account for cardiac motion have been applied to the study of aortic flow patterns via CFD. Cardiac motion seems to be most prevalent in altering ascending aortic (AAo) flow rather than flow in the arch or descending aortic flow, likely due in part to less tissue tethering for AAo than the descending aorta [46]. Differences in time-averaged WSS quantified in this study from simulations with the measured PC-MRI inflow waveforms, as compared to motion-compensated cardiac waveforms, were more pronounced than differences from the model creation or mesh dependent aspects of CFD discussed above. These results suggest that accounting for cardiac motion when quantifying blood flow through the aortic valve can lead to different conclusions for hemodynamic indices, which may be important, if these results are ultimately used to predict patient outcomes [46]. CFD modeling may, thus, aid in optimal management of aortic and aortic arch diseases—whether by influencing operative technique or optimizing devices through material development.

Modeling can aid analysis of aortic dilation, which occurs in patients with bicuspid aortic valves, or in those with connective tissue diseases, such as Marfan, Loeys-Dietz, and Ehlers Danlos syndromes. It is unclear if this is causal, or, more likely, contributing to the underlying vascular pathology. In these populations, CFD has demonstrated adversely high OSI in the ascending aorta, an area prone to dilation [62]. Many of these patients undergo an operation to treat an excessively dilated aorta, in order to prevent aortic rupture. Operative techniques

used might include total aortic root and valve replacement (TAR), valve-sparing root replacement (VSRR), or the novel and less invasive procedure of placing a personalized external aortic root support (PEARS) introduced by Golesworthy et al. [63]. Using MRI-derived data for CFD modeling, Marfan patients have recently been studied after operation for placement of PEARS, and although qualitative hemodynamic indices appeared similar, some small differences in quantitative measures of helical flow were seen pre- and post PEARS in a small cohort. Larger, longitudinal studies will be needed to understand the hemodynamic effects of these operations. CFD may be used in the future to optimize therapy [64] by aiding the creation of aortic "sleeves" from materials which impart better WSS properties to the patients.
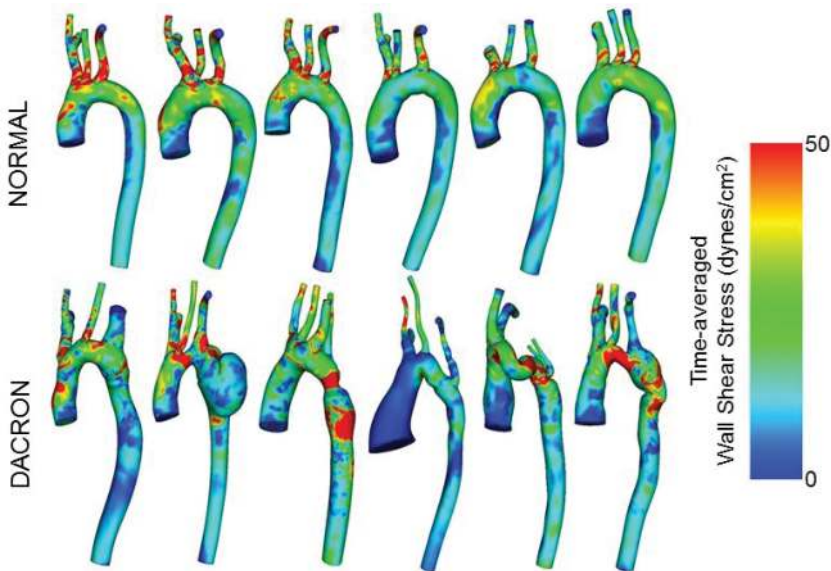

Figure 10. CFD for arch repair by Dacron patch. Time-averaged WSS distributions in six normal subjects (top, 5M, 1F ages 25–33 years) as well as age- and gender-matched patients previously treated for CoA by Dacron patch aortoplasty (below).

3.2. Single ventricle CFD modeling

Over the last decade, CFD modeling has increasingly been applied to patients with single ventricle physiology (**Table 3**), who often require multiple palliative operations in infancy and childhood. The goal of operative therapy is to have the functioning ventricle as the systemic pump, and to secure a source of pulmonary blood flow. Unobstructed flow to the systemic and pulmonary circulations is the goal—to achieve widely patent branch pulmonary arteries and no residual aortic arch obstruction [65].

When the aorta is small, as in hypoplastic left heart syndrome (HLHS), shortly after birth, the infant is palliated with a Norwood operation to create a neo-aorta from side-side anastomosis

of the main pulmonary artery (MPA) and native aorta. Usually, arch repair is undertaken in the same setting. Atrial septectomy occurs too - to allow mixing of systemic and pulmonary venous flow, and pulmonary flow is guaranteed by either an aortopulmonary arterial shunt (i.e., either a Blalock-Taussig (BT) or a central shunt) or right ventricular (RV) to pulmonary shunt (i.e., the Sano shunt). Some time between 3 and 6 months' of age, when the pulmonary vascular resistance is acceptable, the patient undergoes cavo-pulmonary shunt (**Figure 11**) to direct a portion of the systemic venous blood to the lungs for oxygenation. Finally, when the child is older (18 months to 4 years of age), the remaining systemic venous blood and hepatic blood are directed to the lungs via completion of the Fontan (**Figure 12**). CMR is often used in clinical follow-up of these patients.

RV morphology	LV morphology	RV or LV morphology
• Hypoplastic left heart syndrome (HLHS)	• Tricuspid atresia	• Unbalanced AV canal defect
• Complex double outlet RV	• Pulmonary atresia	• Straddling or criss-cross AV valve connections
	• Doublet inlet LV	• Heterotaxy
	• Severe Epstein's anomaly	

With permission from Johnson et al. [65].

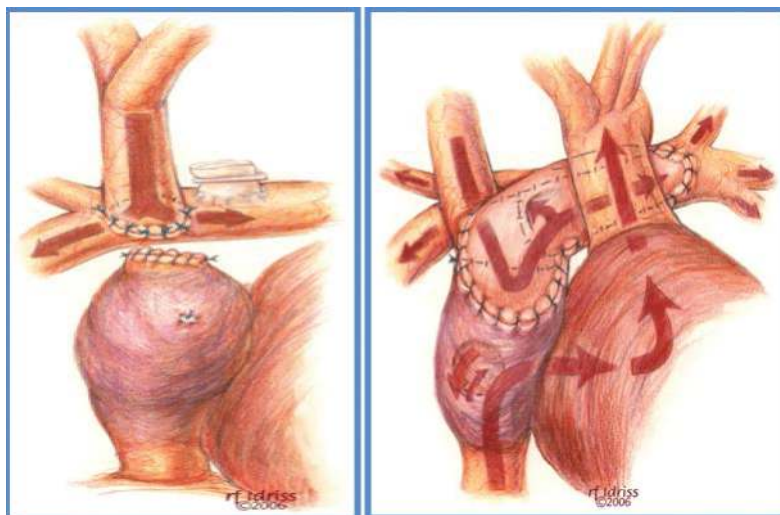**Table 3.** Single ventricular anatomy [65].

Figure 11. Cavo-pulmonary shunts of the Glenn circuit (left, current era) and Hemi-Fontan (right, original operative technique [66]. With permission from Pelletier et al. CTSNet.org. 2013.
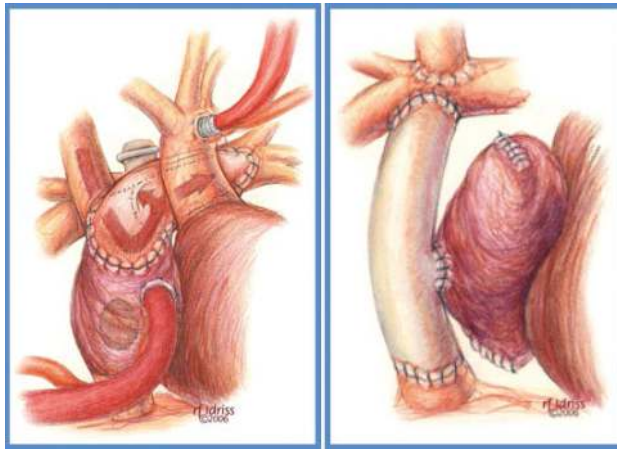
Figure 12. Fontan circulations—various adaptations. "Classic Fontan" (left) has a "classic Glenn circuit" plus an anastomosis of the right atrial appendage to the left pulmonary artery (LPA). Lateral tunnel Fontan (not shown) uses a baffle within the right atrium to partition systemic and pulmonary venous blood, allowing for child's growth. Extracardiac conduit Fontan (right) uses a tube graft to connect IVC to Glenn (SVC/PA), and is often fenestrated [67]. With permission from Jacobs et al. CTSNet.org. 2013.

Using CMR data, CFD modeling in single ventricle patients has focused on understanding energy losses occurring in these unique low-velocity flow Glenn and Fontan circuits. Modeling has aimed to understand blood flow distribution to the lungs by using branch pulmonary arterial PC-MRI data in CFD models. In this manner, CFD has also led to a better understanding of the pulmonary distribution of hepatic flow and the elusive "hepatic factor" which has been implicated in the development of pulmonary arteriovenous malformations [68–72].

Catheterization-based CFD modeling, such as that included in the work by Migliavacca et al. [73], has advanced the clinicians' understanding of the unique Norwood circulation by showing that (1) larger shunts diverted an increased proportion of cardiac output to the lungs and away from systemic perfusion, resulting in poorer oxygen delivery and pulmonary overcirculation, and that (2) the systemic vascular resistance exerted more effects on hemodynamics than pulmonary vascular resistance. CMR-based CFD modeling efforts have been less common in this Norwood population, because of a number of challenges. First, highly turbulent flow from shunts (BT, central or Sano) can lead to inaccuracies in modeling, because of suboptimal PC-MRI data. Second, as this Norwood population is very young ages (i.e., neonates to a few months of age), often 3D anatomic imaging data (CMR or CT) are not readily available, as it is not typically acquired during routine clinical care, which relies predominantly on echocardiographic data. Finally, without catheterization data simultaneous with 3D anatomic imaging, accurate pulmonary and systemic resistance data may not be available, thereby leading to inaccuracies in CFD modeling. Furthermore, the influences of anesthesia (used during catheterization or 3D image acquisition) on such resistance data may lead to models that may not adequately represent real-life clinical conditions. Nonetheless, computational modeling of

this unique Norwood physiology has been attempted and refined over the last two decades [74] with a nice review of the challenges provided by Pennati et al. [75].

CFD modeling of cavo-pulmonary shunts has been more limited relative to the CFD study of the total cavo-pulmonary shunt (Fontan). In pilot research, the Stanford Institute for Computational and Mathematical Engineering, though, systematically studied five Glenn patients, incorporating CMR data and catheterization data into their CFD models. Inflow data came from the superior vena cava (SVC) PC-MRI flow data, while outflow data were more complex and depended on the patient's specific pulmonary tree. They first determined right and left lung flow split from the right pulmonary artery (RPA) and the left pulmonary artery (LPA) PC-MRI flow data and then determined the total resistance—i.e., R_p (proximal resistance) plus R_d (distal resistance) for the pulmonary tree. They calculated the mean flow in each branch as being proportional to the outlet surface area and calculated the downstream resistance by the mean pressure gradient (obtained at catheterization) between SVC and left atrium. The authors show low WSS, complex Glenn flow patterns at the caval-pulmonary anastomoses with a transition to laminar flow more distally in the lung, and a complex pressure waveform which dampens after the anastomoses. Power loss in this small cohort was low, and the efficiency of flow was high. The complexity of the pulmonary tree seems to add computational time, but more work is needed to understand how many pulmonary branches should be modeled for accuracy. This study highlights the complexity of assigning appropriate inlet and outlet boundary conditions—a problem that is compounded when patients are studied by either CMR or cardiac catheterization while they are under anesthesia which alters systemic and pulmonary resistances [76].

CFD may be useful for bilateral bidirectional Glenn connections [77], where patients have the persistence of the left and right superior vena cava. Case reports of CFD modeling in this unique Glenn circuit show differential lung flow due to differences in pulmonary resistance (which may result, e.g., from unilateral lung disease (e.g., pneumonia)) or differences in branch pulmonary arterial dimensions. Furthermore, de Zelicourt et al. [78] have noted that unbalanced lung perfusion may affect pulmonary arterial growth. Thus, constructing the best Glenn circuit with attention to downstream branch pulmonary arterial flow may be essential to long-term patient health.

Surgeons have always tried to avoid "right angles" in the construct of the unique bidirectional Glenn and Fontan circuits, as they perceived unfavorable flow disturbances in these regions. de Leval et al. [79, 80] described various methods for palliation of HLHS. In 2007, Bove et al. [81] studied Fontan circuits of different varieties using computational simulations and showed that when either the total cavo-pulmonary connection (TCPC) or the extra cardiac connection (ECC) is performed after a bidirectional Glenn anastomosis, caval offset of the superior and inferior vena cavae (IVC) can be achieved by beveling the IVC portion of the connection to either the right or the left lung. They demonstrated that beveling the TCPC to the right conferred a significant advantage to the TCPC. Similarly, when the ECC was beveled toward the left lung, important differences were found in flow distribution, but not power losses. This research has been continued by many with continued scrutiny regarding possible power losses in this low-velocity circuit, which is prone to swirling of blood flow due to competitive flow

from the superior and inferior vena cavae [81, 82]. Some centers, such as the Children's Hospital of Philadelphia and Stanford University, among others, have conducted "virtual operative procedures" to study the hemodynamic effects of a given operation by employing CMR-based CFD modeling techniques. These computations have led some to alter the Fontan circuit by employing a "Y graft" for the Fontan [83], as first described by two groups—Marsden et al. [84] and Soerensen et al. [85]. Not only is the energy loss reduced, especially during simulated exercise, but also IVC flow (and the seemingly critical "hepatic flow") can be more equally distributed to the right and left lung fields, which is potentially protective against the development of pulmonary arteriovenous malformations (**Figure 13**) [83, 85, 86].
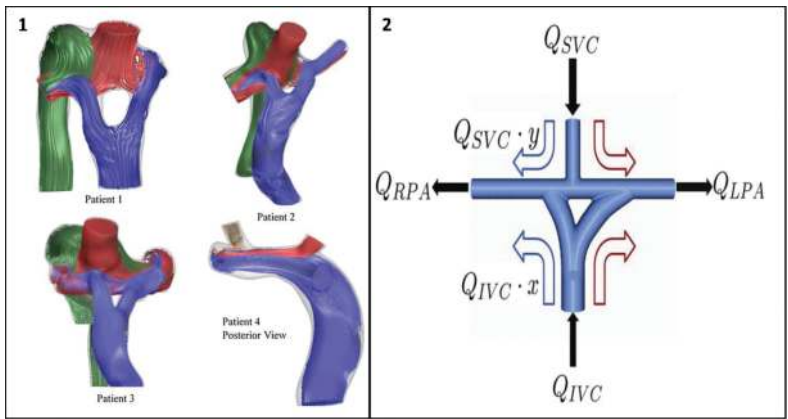

Figure 13. A novel variation in Fontan circuit [83, 86]. Panel 1 shows color representations of the blood flow from azygous vein (green), Glenn circuit (red), and inferior vena cava into the two arms of the Fontan Y graft (blue). Panel 2 gives blood flow calculations for this "Y graft", based on conservation of mass; thus, QRPA = QIVC • x + QSVC • y and QLPA = QIVC • $(1 - x)$ + QSVC • $(1 - y)$, where x is the fraction of hepatic flow going to the RPA and y is the fraction of SVC flow going to the RPA (SVC, superior vena cava; IVC, inferior vena cava; RPA, right pulmonary artery; LPA, left pulmonary artery; Q, flow rate). With permission and adapted from Haggerty et al. [83] and Yang et al. [86].

3.3. Tetralogy of Fallot CFD modeling

Patients with Tetralogy of Fallot (TOF) (i.e., subpulmonary and/or pulmonary valve stenosis with ventricular septal defect, overriding aorta, and right ventricular (RV) hypertrophy) typically undergo operative repair in infancy. Long term, their outcome is related to the degree of chronic pulmonary regurgitation (PR) (i.e., pulmonary valve leakage), and resulting RV dilation and RV dysfunction. Restrictive RV physiology correlates with larger RV and more PR after repair [87]. Pulmonary arterial compliance impacts the amount of regurgitation [88]. Thus, establishing and maintaining appropriate sized branch pulmonary arteries is essential, as elevated resistance distal to compliant arteries exacerbates PR. Furthermore, the initial type of TOF repair may impact how much PR a patient has—with those having RV outflow tract (RVOT) transannular patches having considerably more PR and more dilated RV than those with RV—pulmonary arterial conduits [89]. Patients with repaired TOF, in the current era, are

frequently studied by CMR to better understand when the PR has progressed sufficiently to warrant operative intervention for pulmonary valve replacement [90].

CMR-based CFD modeling has been applied to the study of TOF patients to understand how branch pulmonary arterial geometry (i.e., diameters and the bifurcation angles for the right and left pulmonary arteries) influences pulmonary regurgitation (**Figure 14**) [91, 92]. Chern et al. found that regurgitation occurs first from the LPA and suggested that it may be due to the small angle between LPA and MPA. The authors acknowledge the limitations of their CFD models which do not account for the influences of either distal pulmonary vascular resistance or ventricular hypertrophy (diastolic pressure) on pulmonary regurgitation.
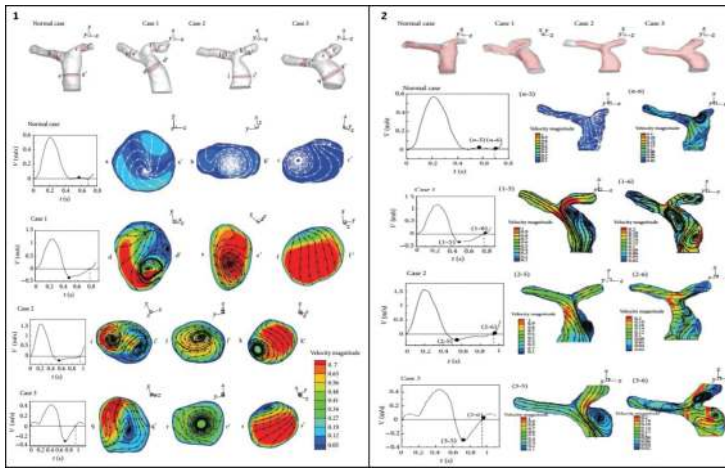

Figure 14. Numerical study of blood flow in pulmonary arteries after repair of Tetralogy of Fallot with different flow patterns in diastole based on angle of bifurcation. 1. Cross-sectional flow patterns and velocity distributions are shown for minimum velocity in the cardiac cycle (as noted by the black dot on the graph). 2. Flow patterns and velocity distributions shown at the minimum flow location and at end diastole (as noted by the black dots on the graph) [93]. With permission and adapted from Chern et al. [93].

Some researchers have proposed that a "reference geometry atlas" be available for the branch pulmonary arteries onto which specific patient data (derived from CMR 3D MRA imaging) may be mapped, so as to reduce computational time [92]. This is a novel idea that may allow CFD to move more readily from the research realm to clinical setting. Others have described in silico models to permit "virtual surgery" for patients with TOF and left pulmonary arterial stenosis [94], an intriguing application that warrants further CFD study with larger cohorts. Another novel application of CFD for patients with repaired TOF is modeling of the RVOT flow to target those for whom transcatheter pulmonary valve replacement is not currently the ideal intervention due to RVOT dilation. In this manner, CFD may aid the design of novel percutaneously placed "pulmonary valve reducer" (for those with enlarged RVOT) [95], thus allowing nonoperative pulmonary valve replacement. Additional CFD research for TOF patients is warranted as better solutions are sought for this population that has chronic PR.

4. Conclusions

In summary, creating clinically relevant CFD models requires care and rigor by individuals at all steps in the process—from initial acquisition of clinical data through all the steps of mathematical modeling. CFD is moving beyond being simply an intriguing mathematical study of blood flow. Based on many pilot studies, CFD is poised to have an increasingly powerful role in the care of patients with CVD in the next decade, by allowing a more refined understanding of the hemodynamics of both acquired CVD due to atherosclerosis and CHD. Continued partnerships between clinician-scientists and engineers are essential to the successful achievement of this goal. Only with such collaborations will the complex process of patient-specific modeling be streamlined and successfully integrated into clinical decision making to optimize medical and interventional therapies for cardiovascular disease.

Acknowledgements

Author details

Margaret M. Samyn[1*] and John F. LaDisa[2]

*Address all correspondence to: msamyn@chw.org

1 Medical College of Wisconsin, Pediatrics (Cardiology), Milwaukee, WI, USA

2 Marquette University, Biomedical Engineering, Milwaukee, WI, USA

References

[1] Mozaffarian D, Benjamin EJ, Go AS, Arnett DK, Blaha MJ, Cushman M, Das SR, de Ferranti S, Després J, Fullerton HJ, Howard VJ, Huffman MD, Isasi CR, Jiménez MC, Judd SE, Kissela BM, Lichtman JH, Lisabeth LD, Liu S, Mackey RH, Magid DJ, McGuire DK, Mohler ER, Moy CS, Muntner P, Mussolino ME, Nasir K, Neumar RW, Nichol G, Palaniappan L, Pandey DK, Reeves MJ, Rodriguez CJ, Rosamond W, Sorlie PD, Stein J, Towfighi A, Turan TN, Virani SS, Woo D, Yeh RW, Turner MB. Heart disease and stroke

statistics—2016 update: a report from the American Heart Association. Circulation. 2016;133:e38–e360. DOI: 10.1161/CIR.0000000000000350.

[2]   2012 European Cardiovascular Disease Statistics [Internet]. 2016. Available from: http://www.escardio.org/The-ESC/Initiatives/EuroHeart/2012-European-Cardiovascular-Disease-Statistics [Accessed: 4/7/2016].

[3]   Marelli A, Gilboa S, Devine O, Kucik J, lonescu-lttu R, Oster M, Riehle-Colarusso T, Correa A, Jenkins K. Estimating the congenital heart disease population in the United States in 2010—what are the numbers? Journal of the American College of Cardiology. 2012;59:E787–E787.

[4]   Wolinsky H, Glagov S. Comparison of abdominal and thoracic aortic medial structure in mammals. Circulation Research. 1969;25:677–686. DOI: 10.1161/01.RES.25.6.677.

[5]   Xu CP, Glagov S, Zatina MA, Zarins CK. Hypertension sustains plaque progression despite reduction of hypercholesterolemia. Hypertension. 1991;18:123–129. DOI: 10.1161/01.HYP.18.2.123.

[6]   Liu SQ, Fung YC. Relationship between hypertension, hypertrophy, and opening angle of zero-stress state of arteries following aortic constriction. Journal of Biomechanical Engineering. 1989;111:325–335. DOI: 10.1115/1.3168386.

[7]   Kleinstreuer C, Hyun S, Buchanan JR Jr, Longest PW, Archie JP Jr, Truskey GA. Hemodynamic parameters and early intimal thickening in branching blood vessels. Critical Reviews in Biomedical Engineering. 2001;29:1–64.

[8]   Ku DN, Giddens DP, Zarins CK, Glagov S. Pulsatile flow and atherosclerosis in the human carotid bifurcation. Positive Correlation between plaque location and low oscillating shear stress. Arteriosclerosis, Thrombosis, and Vascular Biology. 1985;5:293–302. DOI: 10.1161/01.ATV.5.3.293.

[9]   Lehoux SS, Tronc F, Tedgui A. Mechanisms of blood flow-induced vascular enlargement. Biorheology. 2002;39:319–324.

[10] Malek AM, Alper SL, Izumo S. Hemodynamic shear stress and its role in atherosclerosis. Journal of the American Medical Association. 1999;282:2035–2042.

[11] Moore JE, Xu C, Glagov S, Zarins CK, Ku DN. Fluid wall shear stress measurements in a model of the human abdominal aorta: oscillatory behavior and relationship to atherosclerosis. Atherosclerosis. 1994;110:225–240. DOI: 10.1016/0021-9150(94)90207-0.

[12] Ojha M. Spatial and temporal variations of wall shear stress within an end-to-side arterial anastomosis model. Journal of Biomechanics. 1993;26:1377–1388. DOI: 10.1016/0021-9290(93)90089-W.

[13] De Nevers N. Fluid Mechanics for Chemical Engineers. 3rd ed. Boston: McGraw-Hill Higher Education; 2005. 632 p.

[14] LaDisa JFJ, Dholakia RJ, Figueroa CA, Vignon-Clementel IE, Chan FP, Samyn MM, Cava JR, Taylor CA, Feinstein JA. Computational simulations demonstrate altered wall shear

stress in aortic coarctation patients treated by resection with end-to-end anastomosis. Congenital Heart Disease. 2011;6:432–443. DOI: 10.1111/j.1747-0803.2011.00553.x.

[15] Müller J, Sahni O, Li X, Jansen KE, Shephard MS, Taylor CA. Anisotropic adaptive finite element method for modelling blood flow. Computer Methods in Biomechanics and Biomedical Engineering. 2005;8:295–305. DOI: 10.1080/10255840500264742.

[16] Sahni O, Müller J, Jansen KE, Shephard MS, Taylor CA. Efficient anisotropic adaptive discretization of the cardiovascular system. Computer Methods in Applied Mechanics and Engineering. 2006;195:5634–5655. DOI: 10.1016/j.cma.2005.10.018.

[17] Nichols W. McDonald's Blood Flow in Arteries: Theoretical, Experimental and Clinical Principles. 5th ed. Boca Raton, FL: CRC Press; 2005. 570 p.

[18] Sankaran S, Esmaily Moghadam M, Kahn AM, Tseng EE, Guccione JM, Marsden AL. Patient-specific multiscale modeling of blood flow for coronary artery bypass graft surgery. Annals of Biomedical Engineering. 2012;40:2228–2242. DOI: 10.1007/s10439-012-0579-3.

[19] Figueroa CA, Vignon-Clementel IE, Jansen KE, Hughes TJR, Taylor CA. A coupled momentum method for modeling blood flow in three-dimensional deformable arteries. Computer Methods in Applied Mechanics and Engineering. 2006;195:5685–5706. DOI: 10.1016/j.cma.2005.11.011.

[20] Lotz J, Meier C, Leppert A, Galanski M. Cardiovascular flow measurement with phase-contrast MR imaging: basic facts and implementation. RadioGraphics. 2002;22:651–671.

[21] Stergiopulos NN, Meister JJ, Westerfhoff N. Simple and accurate way for estimating total and segmental arterial compliance: the pulse pressure method. Annals of Biomedical Engineering. 1994;22:392–397.

[22] Stergiopulos NS. Use of pulse pressure method for estimating total arterial compliance in vivo. American Journal of Physiology—Heart and Circulatory Physiology. 1999;276:H424–H428.

[23] Samyn M, Dholakia R, Wang H, Co-Vu J, Yan K, Widlansky M, LaDisa J, Simpson P, Alemzadeh R. Cardiovascular magnetic resonance imaging-based computational fluid dynamics/fluid structure interaction pilot study to detect early vascular changes in pediatric patients with Type 1 diabetes. Pediatric Cardiology. 2015;36:851–861. DOI: 10.1007/s00246-014-1071-7.

[24] Kilner PJ, Yang GZ, Mohiaddin RH, Firmin DN, Longmore DB. Helical and retrograde secondary flow patterns in the aortic arch studied by three-directional magnetic resonance velocity mapping. Circulation. 1993;88:2235–2247.

[25] Liu X, Sun A, Fan Y, Deng X. Physiological significance of helical flow in the arterial system and its potential clinical applications. Annals of Biomedical Engineering. 2015;43:3–15. DOI: 10.1007/s10439-014-1097-2.

[26] Niezen RA, Doornbos J, van der Wall EE, de Roos A. Measurement of aortic and pulmonary flow with MRI at rest and during physical exercise. Journal of Computer Assisted Tomography. 1998;22:194–201.

[27] Weber TF, von Tengg-Kobligk H, Kopp-Schneider A, Ley-Zaporozhan J, Kauczor H, Ley S. High-Resolution phase-contrast MRI of aortic and pulmonary blood flow during rest and physical exercise using a MRI compatible bicycle ergometer. European Journal of Radiology. 2011;80:103–108. DOI: 10.1016/j.ejrad.2010.06.045.

[28] Pedersen EM, Kozerke S, Ringgaard S, Scheidegger MB, Boesiger P. Quantitative abdominal aortic flow measurements at controlled levels of ergometer exercise. Magnetic Resonance Imaging. 1999;17:489–494. DOI: 10.1016/S0730-725X(98)00209-4.

[29] Steeden JA, Atkinson D, Taylor AM, Muthurangu V. Assessing vascular response to exercise using a combination of real-time spiral phase contrast MR and noninvasive blood pressure measurements. Journal of Magnetic Resonance Imaging. 2010;31:997–1003. DOI: 10.1002/jmri.22105.

[30] Sampath S, Derbyshire JA, Ledesma-Carbayo MJ, McVeigh ER. Imaging left ventricular tissue mechanics and hemodynamics during supine bicycle exercise using a combined tagging and phase-contrast MRI pulse sequence. Magnetic Resonance in Medicine. 2011;65:51–59. DOI: 10.1002/mrm.22668.

[31] Taylor CA, Cheng CP, Espinosa LA, Tang BT, Parker D, Herfkens RJ. In vivo quantification of blood flow and wall shear stress in the human abdominal aorta during lower limb exercise. Annals of Biomedical Engineering. 30:402–408. DOI: 10.1114/1.1476016.

[32] Cheng CP, Schwandt DF, Topp EL, Anderson JH, Herfkens RJ, Taylor CA. Dynamic exercise imaging with an MR-compatible stationary cycle within the general electric open magnet. Magnetic Resonance in Medicine. 2003;49:581–585. DOI: 10.1002/mrm.10364.

[33] Cheng CP, Herfkens RJ, Lightner AL, Taylor CA, Feinstein JA. Blood flow conditions in the proximal pulmonary arteries and vena cavae: healthy children during upright cycling exercise. American Journal of Physiology–Heart and Circulatory Physiology. 2004;287:H921–H926. DOI: 10.1152/ajpheart.00022.2004.

[34] Kim HJ, Vignon-Clementel I, Figueroa CA, LaDisa JF, Jansen KE, Feinstein JA, Taylor CA. On coupling a lumped parameter heart model and a three-dimensional finite element aorta model. Annals of Biomedical Engineering. 2009;37:2153–2169. DOI: 10.1007/s10439-009-9760-8.

[35] LaDisa JFJ, Figueroa CA, Vignon-Clementel I, Kim HJ, Xiao N, Ellwein LM, Chan FP, Feinstein JA, Taylor CA. Computational simulations for aortic coarctation: representative results from a sampling of patients. Journal of Biomechanical Engineering. 2011;133:091008–091008.

[36] Ellwein L, Samyn MM, Danduran M, Schindler-Ivens S, Liebham S, LaDisa Jr. JF. Toward translating near-infrared spectroscopy oxygen saturation data for the non-

invasive predication of spatial and temporal hemodynamics during exercise. Biomechanics and Modeling in Mechanobiology. 2016 [Epub ahead of print].

[37] Frydrychowicz A, Stalder AF, Russe MF, Bock J, Bauer S, Harloff A, Berger A, Langer M, Hennig J, Markl M. Three-dimensional analysis of segmental wall shear stress in the aorta by flow-sensitive four-dimensional-MRI. Journal of Magnetic Resonance Imaging. 2009;30:77–84. DOI: 10.1002/jmri.21790.

[38] Wentzel JJ, Corti R, Fayad ZA, Wisdom P, Macaluso F, Winkelman MO, Fuster V, Badimon JJ. Does shear stress modulate both plaque progression and regression in the thoracic aorta?: Human study using serial magnetic resonance imaging. Journal of the American College of Cardiology. 2005;45:846–854. DOI: 10.1016/j.jacc.2004.12.026.

[39] LaDisa JF, Olson LE, Guler I, Hettrick DA, Kersten JR, Warltier DC, Pagel PS. Circumferential vascular deformation after stent implantation alters wall shear stress evaluated with time-dependent 3D computational fluid dynamics models. Journal of Applied Physiology. 2005;98:947–957. DOI: 10.1152/japplphysiol.00872.2004.

[40] White CR, Haidekker M, Bao X, Frangos JA. Temporal gradients in shear, but not spatial gradients, stimulate endothelial cell proliferation. Circulation. 2001;103:2508–2513.

[41] Hope MD, Meadows AK, Hope TA, Ordovas KG, Saloner D, Reddy GP, Alley MT, Higgins CB. Clinical evaluation of aortic coarctation with 4D flow MR imaging. Journal of Magnetic Resonance Imaging. 2010;31:711–718. DOI: 10.1002/jmri.22083.

[42] Markl M, Kilner PJ, Ebbers T. Comprehensive 4D velocity mapping of the heart and great vessels by cardiovascular magnetic resonance. Journal of Cardiovascular Magnetic Resonance. 2011;13:1–22. DOI: 10.1186/1532-429X-13-7.

[43] Barker AJ, Markl M, Bürk J, Lorenz R, Bock J, Bauer S, Schulz-Menger J, von Knobelsdorff-Brenkenhoff F. Bicuspid aortic valve is associated with altered wall shear stress in the ascending aorta. Circulation: Cardiovascular Imaging. 2012;5:457–466.

[44] Bieging ET, Frydrychowicz A, Wentland A, Landgraf BR, Johnson KM, Wieben O, François CJ. In vivo three-dimensional MR wall shear stress estimation in ascending aortic dilatation. Journal of Magnetic Resonance Imaging. 2011;33:589–597. DOI: 10.1002/jmri.22485.

[45] van Ooij P, Potters WV, Nederveen AJ, Allen BD, Collins J, Carr J, Malaisrie SC, Markl M, Barker AJ. A methodology to detect abnormal relative wall shear stress on the full surface of the thoracic aorta using four-dimensional flow MRI. Magnetic Resonance in Medicine. 2015;73:1216–1227. DOI: 10.1002/mrm.25224.

[46] Wendell DC, Samyn MM, Cava JR, Krolikowski MM, LaDisa JF. The impact of cardiac motion on aortic valve flow used in computational simulations of the thoracic aorta. Journal of Biomechanical Engineering. 2016;138(9) DOI: 10.1115/1.4033964.

[47] Morris PD, Narracott A, von Tengg-Kobligk H, Silva Soto DA, Hsiao S, Lungu A, Evans P, Bressloff NW, Lawford PV, Hose DR, Gunn JP. Computational fluid dynamics

modelling in cardiovascular medicine. Heart. 2016;102:18–28. DOI: 10.1136/ heartjnl-2015-308044.

[48] Libby P. The vascular biology of atherosclerosis. In: Mann DL, Zipes DP, Libby P, Bonow RO, editors. Braunwald's Heart Disease: A Textbook of Cardiovascular Medicine. 10th ed. Philadelphia, PA: Elsevier Health Sciences; 2014. p. 873–890.

[49] Berenson GS, Srnivasan SR. Cardiovascular risk factors in youth with implications for aging: the bogalusa heart study. Neurobiology of Aging. 2005;26:303–307. DOI: 10.1016/ j.neurobiolaging.2004.05.009.

[50] Juonala M, Magnussen CG, Venn A, Dwyer T, Burns TL, Davis PH, Chen W, Srinivasan SR, Daniels SR, Kähönen M, Laitinen T, Taittonen L, Berenson GS, Viikari JSA, Raitakari OT. Influence of age on associations between childhood risk factors and carotid intima-media thickness in adulthood: The Cardiovascular Risk in Young Finns Study, the Childhood Determinants of Adult Health Study, the Bogalusa Heart Study, and the Muscatine Study for the International Childhood Cardiovascular Cohort (i3C) Consortium. Circulation. 2010;122:2514–2520. DOI: 10.1161/CIRCULATIONAHA. 110.966465.

[51] Tracy RE, Newman WPI, Wattigney WA, Berenson GS. Risk factors and atherosclerosis in youth autopsy findings of the Bogalusa Heart Study. American Journal of the Medical Sciences. 1995;310:S42.

[52] Glagov S, Weisenberg E, Zarins CK, Stankunavicius R, Kolettis GJ. Compensatory enlargement of human atherosclerotic coronary arteries. New England Journal of Medicine. 1987;316:1371–1375. DOI: 10.1056/NEJM198705283162204.

[53] Katranas SA, Antoniadis AP, Kelekis AL, Giannoglou GD. Insights on atherosclerosis by non-invasive assessment of wall stress and arterial morphology along the length of human coronary plaques. The International Journal of Cardiovascular Imaging. 2015;31:1627–1633. DOI: 10.1007/s10554-015-0736-5.

[54] LaDisa JF, Bowers M, Harmann L, Prost R, Doppalapudi AV, Mohyuddin T, Zaidat O, Migrino RQ. Time-efficient patient-specific quantification of regional carotid artery fluid dynamics and spatial correlation with plaque burden. Medical Physics. 2010;37:784–792. DOI: 10.1118/1.3292631.

[55] Babar GS, Zidan H, Widlansky ME, Das E, Hoffmann RG, Daoud M, Alemzadeh R. Impaired endothelial function in preadolescent children with Type 1 DIABETES. Diabetes Care. 2011;34:681–685. DOI: 10.2337/dc10-2134.

[56] Pasterkamp G, Galis ZS, de Kleijn DPV. Expansive arterial remodeling: location, location, location. Arteriosclerosis, Thrombosis, and Vascular Biology. 2004;24:650–657. DOI: 10.1161/01.ATV.0000120376.09047.fe.

[57] Brown JW, Ruzmetov M, Hoyer MH, Rodefeld MD, Turrentine MW. Recurrent coarctation: is surgical repair of recurrent coarctation of the aorta safe and effective?

The Annals of Thoracic Surgery. 2009;88:1923–1931. DOI: 10.1016/j.athoracsur. 2009.07.024.

[58] Kron IL, Flanagan TL, Rheuban KS, Carpenter MA, Gutgesell HPJ, Blackbourne LH, Nolan SP. Incidence and risk of reintervention after coarctation repair. Annals of Thoracic Surgery. 1990;49:920–926.

[59] Kavey RW, Allada V, Daniels SR, Hayman LL, McCrindle BW, Newburger JW, Parekh RS, Steinberger J. Cardiovascular risk reduction in high-risk pediatric patients: a scientific statement from the American Heart Association Expert Panel on Population and Prevention Science; the Councils on Cardiovascular Disease in the Young, Epidemiology and Prevention, Nutrition, Physical Activity and Metabolism, High Blood Pressure Research, Cardiovascular Nursing, and the Kidney in Heart Disease; and the Interdisciplinary Working Group on Quality of Care and Outcomes Research: Endorsed by the American Academy of Pediatrics. Circulation. 2006;114:2710–2738. DOI: 10.1161/CIRCULATIONAHA. 106.179568.

[60] Dholakia, Ronak J. Numerical modeling of hemodynamics in the thoracic aorta and alterations by dacron patch treatment of aortic coarctation [Thesis]. Milwaukee: Marquette University; 2009.

[61] Wendell DC, Samyn MM, Cava JR, Ellwein LM, Krolikowski MM, Gandy KL, Pelech AN, Shadden SC, LaDisa Jr. JF. Including aortic valve morphology in computational fluid dynamics simulations: initial findings and application to aortic coarctation. Medical Engineering & Physics. 2013;35:723–735. DOI: 10.1016/j.medengphy. 2012.07.015.

[62] Camarda JA, Earing MG, Dholakia RJ, Wang H, Kwon S, LaDisa JF, Samyn MM. Biophysical properties of the aorta in patients with marfan syndrome and related connective tissue disorders: evaluation with MRI and computational fluid dynamics modeling. Journal of Cardiovascular Magnetic Resonance. 2011;13:P219.

[63] Golesworthy T, Lampérth M, Mohiaddin R, Pepper J, Thornton W, Treasure T. The tailor of gloucester: a jacket for the Marfan's aorta. The Lancet. 364:1582. DOI: 10.1016/ S0140-6736(04)17308-X.

[64] Singh SD, Xu XY, Wood NB, Pepper JR, Izgi C, Treasure T, Mohiaddin RH. Aortic flow patterns before and after personalised external aortic root support implantation in Marfan patients. Journal of Biomechanics. 2016;49:100–111. DOI: 10.1016/j.jbiomech. 2015.11.040.

[65] Johnson TR, Samyn MM, Sena L. Cardiac CT and MR evaluation of the adult Fontan patient. In: Saremi F, editor. Cardiac CT and MR for Adult Congenital Heart Disease New York: Springer Science & Business Media; 2013. p. 481–498. DOI: 10.1007/978-1-4614-8875-0.

[66] Superior Cavopulmonary Anastomosis: The Hemi-Fontan and Bidirectional Glenn [Internet]. 2016. Available from: http://www.ctsnet.org/article/superior-cavopulmonary-anastomosis-hemi-fontan-and-bidirectional-glenn [Accessed: 4/12/2016].

[67] Modified Fontan [Internet]. 2016. Available from: http://www.ctsnet.org/article/modified-fontan [Accessed: 4/12/2016].

[68] Tang E, Yoganathan AP. Optimizing hepatic flow distribution with the Fontan Y-Graft: lessons from computational simulations. The Journal of Thoracic and Cardiovascular Surgery. 2015;149:255–256. DOI: 10.1016/j.jtcvs.2014.09.094.

[69] Pike NA, Vricella LA, Feinstein JA, Black MD, Reitz BA. Regression of severe pulmonary arteriovenous malformations after Fontan revision and "hepatic factor" rerouting. The Annals of Thoracic Surgery. 2004;78:697–699. DOI: 10.1016/j.athoracsur.2004.02.003.

[70] Srivastava D, Preminger T, Lock JE, Mandell V, Keane JF, Mayer JE, Kozakewich H, Spevak PJ. Hepatic venous blood and the development of pulmonary arteriovenous malformations in congenital heart disease. Circulation. 1995;92:1217–1222. DOI: 10.1161/01.CIR.92.5.1217.

[71] Knight WB, Mee RBB. A cure for pulmonary arteriovenous fistulas? The Annals of Thoracic Surgery. 1995;59:999–1001. DOI: 10.1016/0003-4975(94)00735-P.

[72] Vettukattil JJ. Pathogenesis of pulmonary arteriovenous malformations: role of hepatopulmonary interactions. Heart. 2002;88:561–563. DOI: 10.1136/heart.88.6.561.

[73] Migliavacca F, Pennati G, Dubini G, Fumero R, Pietrabissa R, Urcelay G, Bove E, Hsia T, deLeval M. Modeling of the Norwood circulation: effects of shunt size, vascular resistances, and heart rate. American Journal of Physiology—Heart and Circulatory Physiology. 2001;280:H2076–2086.

[74] Biglino G, Giardini A, Hsia T, Figliola R, Taylor AM, Schievano S. Modelling single ventricle physiology: review of engineering tools to study first stage palliation of hypoplastic left heart syndrome. Frontiers in Pediatrics. 2013;1. DOI: 10.3389/fped.2013.00031.

[75] Pennati G, Corsini C, Hsia T, Migliavacca F. computational fluid dynamics models and congenital heart diseases. Frontiers in Pediatrics. 2013;1(4). DOI: 10.3389/fped.2013.00004.

[76] Troianowski G, Taylor CA, Feinstein JA, Vignon-Clementel I. Three-dimensional simulations in glenn patients: clinically based boundary conditions, hemodynamic results and sensitivity to input data. Journal of Biomechanical Engineering. 2011;133:111006–111006. DOI: 10.1115/1.4005377.

[77] Sun Q, Wan D, Liu J, Hong H, Liu Y, Zhu M. Patient-specific computational fluid dynamic simulation of a bilateral bidirectional glenn connection. Medical & Biological Engineering & Computing. 2008;46:1153–1159. DOI: 10.1007/s11517-008-0376-1.

[78] de Zélicourt DA, Pekkan K, Parks J, Kanter K, Fogel M, Yoganathan AP. Flow Study of an extracardiac connection with persistent left superior vena cava. The Journal of Thoracic and Cardiovascular Surgery. 2006;131:785–791. DOI: 10.1016/j.jtcvs. 2005.11.031.

[79] de Leval MR, Dubini G, Migliavacca F, Jalali H, Camporini G, Redington A, Pietrabissa R. Use of Computational fluid dynamics in the design of surgical procedures: application to the study of competitive flows in cavopulmonary connections. The Journal of Thoracic and Cardiovascular Surgery. 1996;111:502–513. DOI: 10.1016/S0022-5223(96)70302-1.

[80] de Leval MR, Kilner PJ, Gewillig M, Bull C. Total cavopulmonary connection: a logical alternative to atriopulmonary connection for complex fontan operations. Experimental Studies and Early Clinical Experience. Journal of Thoracic and Cardiovascular Surgery. 1988;96:682–95.

[81] Bove EL, de Leval MR, Migliavacca F, Balossino R, Dubini G. Toward optimal hemodynamics: computer modeling of the fontan circuit. Pediatric Cardiology. 2007;28:477–481. DOI: 10.1007/s00246-007-9009-y".

[82] de Zélicourt DA, Haggerty CM, Sundareswaran KS, Whited BS, Rossignac JR, Kanter KR, Gaynor JW, Spray TL, Sotiropoulos F, Fogel MA, Yoganathan AP. Individualized computer-based surgical planning to address pulmonary arteriovenous malformations in patients with a single ventricle with an interrupted inferior vena cava and azygous continuation. The Journal of Thoracic and Cardiovascular Surgery. 2011;141:1170–1177. DOI: 10.1016/j.jtcvs.2010.11.032.

[83] Haggerty CM, de Zélicourt DA, Restrepo M, Rossignac J, Spray TL, Kanter KR, Fogel MA, Yoganathan AP. Comparing pre- and post-operative Fontan hemodynamic simulations: implications for the reliability of surgical planning. Annals of Biomedical Engineering. 2012;40:2639–2651. DOI: 10.1007/s10439-012-0614-4.

[84] Marsden AL, Bernstein AJ, Reddy VM, Shadden SC, Spilker RL, Chan FP, Taylor CA, Feinstein JA. Evaluation of a novel Y-shaped extracardiac Fontan Baffle using computational fluid dynamics. The Journal of Thoracic and Cardiovascular Surgery. 2009;137:394–403.e2. DOI: 10.1016/j.jtcvs.2008.06.043.

[85] Soerensen DD, Pekkan K, de Zélicourt D, Sharma S, Kanter K, Fogel M, Yoganathan AP. Introduction of a new optimized total cavopulmonary connection. The Annals of Thoracic Surgery. 2007;83:2182–2190. DOI: 10.1016/j.athoracsur.2006.12.079.

[86] Yang W, Vignon-Clementel IE, Troianowski G, Reddy VM, Feinstein JA, Marsden AL. Hepatic blood flow distribution and performance in conventional and novel Y-graft Fontan geometries: a case series computational fluid dynamics study. The Journal of Thoracic and Cardiovascular Surgery. 2012;143:1086–1097. DOI: 10.1016/j.jtcvs. 2011.06.042.

[87] Samyn MM, Kwon EN, Gorentz JS, Yan K, Danduran MJ, Cava JR, Simpson PM, Frommelt PC, Tweddell JS. Restrictive versus nonrestrictive physiology following

repair of Tetralogy of Fallot: is there a difference? Journal of the American Society of Echocardiography. 2013;26:746–755. DOI: 10.1016/j.echo.2013.03.019.

[88] Kilner PJ, Balossino R, Dubini G, Babu-Narayan SV, Taylor AM, Pennati G, Migliavacca F. Pulmonary regurgitation: the effects of varying pulmonary artery compliance, and of increased resistance proximal or distal to the compliance. International Journal of Cardiology. 2009;133:157–166. DOI: 10.1016/j.ijcard.2008.06.078.

[89] Samyn MM, Powell AJ, Garg R, Sena L, Geva T. Range of ventricular dimensions and function by steady-state free precession cine MRI in repaired Tetralogy of Fallot: right ventricular outflow tract patch vs. conduit repair. Journal of Magnetic Resonance Imaging. 2007;26:934–940.

[90] Geva T. Indications for pulmonary valve replacement in repaired Tetralogy of Fallot: the quest continues. Circulation. 2013;128:1855–1857. DOI: 10.1161/CIRCULATIONA-HA.113.005878.

[91] Chern M, Wu M, Wang H. Numerical investigation of regurgitation phenomena in pulmonary arteries of Tetralogy of Fallot patients after repair. Journal of Biomechanics. 2008;41:3002–3009. DOI: 10.1016/j.jbiomech.2008.07.017.

[92] Guibert R, McLeod K, Caiazzo A, Mansi T, Fernández MA, Sermesant M, Pennec X, Vignon-Clementel IE, Boudjemline Y, Gerbeau J. Group-wise construction of reduced models for understanding and characterization of pulmonary blood flows from medical images. Medical Image Analysis. 2014;18:63–82. DOI: 10.1016/j.media.2013.09.003.

[93] Chern M, Wu M, Her S. Numerical study for blood flow in pulmonary arteries after repair of Tetralogy of Fallot. Computational and Mathematical Methods in Medicine 2012;198108:04/13/2016 DOI: 10.1155/2012/198108.

[94] Rao AS, Menon PG. Presurgical planning using image-based in silico anatomical and functional characterization of Tetralogy of Fallot with associated anomalies. Interactive Cardiovascular and Thoracic Surgery. 2015;20:149–156. DOI: 10.1093/icvts/ivu368.

[95] Caiazzo A, Guibert R, Vignon-Clementel I. A reduced-order modeling for efficient design study of artificial valve in enlarged ventricular outflow tracts. Computer Methods in Biomechanics and Biomedical Engineering. 2016;19(12):1314–1318. DOI: 10.1080/10255842.2015.1133811.